Measurement of photon mass attenuation coefficients

Matthew Krupcale, Calvin Gao
Department of Physics, Case Western Reserve University, Cleveland Ohio, 44106-7079
30 September 2012

Abstract

Gamma radiation passing through a material can be absorbed or scattered, attenuating the incident radiation exponentially with distance. Radioactive isotopes were used to generate monenergetic γ-rays in the range of $31\ \mathrm{keV}$ to $1.332\ \mathrm{MeV}$, which passed through a collimator with an absorption material and detected with a NaI scintillation detector. The photon mass attenuation coefficients were determined for aluminum, copper and lead absorbers as a function of incident γ-ray energy by comparison of energy spectra with the absorber to the energy spectra without the absorber. The aluminum attenuation coefficients agreed with the reference data, having a reduced Chi-squared of $\bar{\chi}^2_{\mathrm{Al}} = 0.36$, while the copper and lead coefficients disagreed with the reference data with reduced Chi-squared values of $\bar{\chi}^2_{\mathrm{Cu}} = 17$ and $\bar{\chi}^2_{\mathrm{Pb}} = 101$, respectively. In the energy range tested, the Compton effect was the dominant scattering mechanism above $662\ \mathrm{keV}$, while the photoelectric effect was dominant below this energy.

Introduction

The purpose of this experiment is to measure the photon mass attenuation coefficient for different absorbers over a range of γ-ray energies and compare the results to previously collected data. General conclusions about the nature of the attenuation process for different absorbers can be made by comparing the results to theory. It is expected that absorbers with large atomic numbers will generally have higher attenuation coefficients at lower energies, and Compton scattering should be the dominant scattering mechanism towards the upper half of the energy range tested. Energy spectra were collected by a multichannel analyzer (MCA) for different γ

sources with and without an absorber. A comparison of the energy peak counts gives a measure of the attenuation coefficients for the absorber at the peak energy.

Theory

The probability of a photon traversing an absorber is proportional to the probability of surviving each of the different kind of reactions. Then for a collimated γ-ray beam of initial intensity I, the residual beam intensity after traversing a distance x through the absorber is [1]

$$S = Ie^{-\lambda x} \tag{1a}$$

where

$$\lambda = n(Z\sigma_c + \sigma_\tau + \sigma_\kappa) \tag{1b}$$

is the linear attenuation coefficient for an atom number density n, atomic number Z, Compton scattering cross-section σ_c, photoelectric absorption cross-section σ_τ and pair-production cross-section σ_κ. We define the mass attenuation coefficient as the linear attenuation coefficient divided by the material density; this quantity is more fundamental because it is independent of the actual density and physical state of the absorber [2]. Then,

$$\mu = \frac{\lambda}{\rho} = \frac{n}{\rho}(Z\sigma_c + \sigma_\tau + \sigma_\kappa) = \frac{N}{M}(Z\sigma_c + \sigma_\tau + \sigma_\kappa) \tag{2}$$

where we have written the number density in terms of Avogadro's constant N and the molar mass M. It is worth noting that the Compton scattering term is roughly material independent, since $\frac{Z}{M} \approx 0.45 \pm 0.05$ for all elements except hydrogen [2].

Apparatus and Methods

The experiment was carried out using a NaI scintillation detector to detect the collimated γ-ray beam and surrounded by lead bricks to shield from background radiation. A high-voltage supply powered the scintillator, and the scintillator signal output was amplified and sent to a

multichannel analyzer for spectrum analysis. A schematic diagram of the experiment setup is shown in Figure 1.

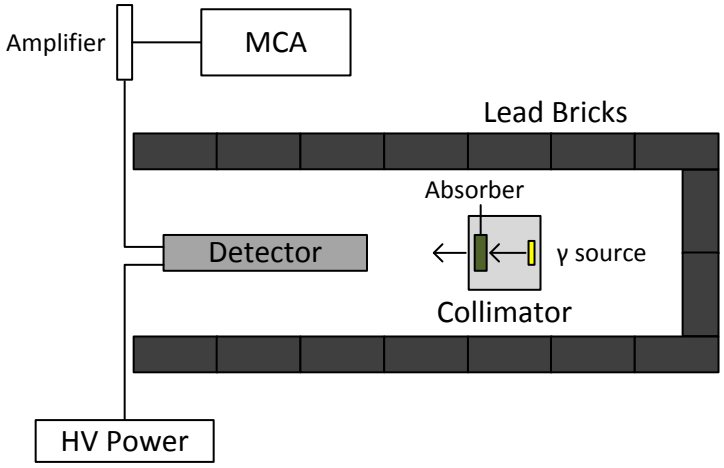

Figure 1 Schematic of experiment setup. The γ source is shown in yellow, and the absorber material is shown in green. The entire arrangement of detector and collimator is surrounded above and on the sides by lead bricks.

Collimating the γ beam reduces the chance of getting secondary interactions of the photons with matter other than the absorber and ensures that the beam is on the same axis as the detector so that photons that pass through the absorber at an angle are not detected. Increasing the distance between the source, absorber and detector will strengthen this effect at the expense of reducing the signal, due to a smaller solid angle of the detector relative to the source. The detector was placed only approximately 10 to 20 cm away from the absorber, and the source was placed roughly 5 to 10 cm away from the absorber. Limitations in the collimator size, amount of shielding and particularly the radioactive source quality prevented the experiment from being much larger.

Sources that were used were chosen based on preliminary measurements of how distinguishable the energy peaks were. The sources were dated in 2002, so majority of the sources were very weak, having undergone several half-lives. See Table 1 for information regarding the sources used. Three absorber materials over a range of atomic numbers were

chosen: aluminum, copper and lead. The sample densities were taken to be the density of a pure absorber material, based on elemental information databases. The absorber thicknesses were measured with a digital caliper of with a precision of 0.01 mm. The aluminum and copper samples were fairly uniform across the surface, resulting in a fairly small deviation in thickness measurement, while the lead sample had a rougher surface and created wider variance in the sample thickness. Table 2 contains information about the absorbers tested.

Table 1 Gamma sources. Radioactive sources were 1 μ Ci solid sealed sources dated from 2002.

Source	Half-life (years)	Energies (keV)
^{60}Co	5.27	1173 1332
^{133}Ba	10.51	31 81 356
^{137}Cs	30.07	32 662

Table 2 Absorber materials. Two different aluminum samples, one copper and one lead sample were tested. Density uncertainty is taken to be one unit of the least significant figure. Thickness uncertainties were estimated by measuring the thickness several times and observing variations in the measurement.

Material	Atomic Number, Z	Density, ρ (g $\cdot$ cm^{-3})	Thickness, x (cm)
Aluminum	13	2.70 ± 0.01	0.313 ± 0.010 0.635 ± 0.010
Copper	29	8.96 ± 0.01	0.630 ± 0.030
Lead	82	11.34 ± 0.01	0.676 ± 0.100

The spectra were first collected for 120 seconds without an absorber, with the aluminum absorber, with the copper absorber and finally with the lead absorber for each radioactive source. A background measurement without any source or absorber in place was taken each time a new source was tested. Calibration of the ORTEC MAESTRO MCA emulation software was done by comparing collected spectra to a reference spectrum for the particular source being used. Once calibrated, the background was subtracted from all of the spectra, and each of the tested energy

peaks were analyzed for their counts above the background level using a Gaussian curve fit technique. Uncertainties in the counts were proportional to the square root of the number of counts, in accordance with Poisson counting statistics.

Results and Analysis

The mass attenuation coefficient was calculated for each absorber and γ-ray source energy using the ratio of number of scintillation pulses counted with the absorber to the ratio without the absorber at a particular γ-ray energy according to [1]

$$\mu = -\frac{1}{x\rho}\ln\left(\frac{S-B}{I-B}\right) \tag{3a}$$

where x is the absorber thickness, ρ is its density, S is the number of counts with the absorber, I is the incident counts without the absorber and B is the background count. Then the uncertainty in the attenuation coefficient in general is (see Appendix for details)

$$\delta_\mu = \frac{1}{x\rho}\sqrt{\left(\ln\left(\frac{S-B}{I-B}\right)\right)^2\left(\left(\frac{\delta_x}{x}\right)^2+\left(\frac{\delta_\rho}{\rho}\right)^2\right)+\left(\frac{\delta_{S-B}}{S-B}\right)^2+\left(\frac{\delta_{I-B}}{I-B}\right)^2} \tag{3b}$$

However, the since the uncertainty in the material density is less than 1%, the density contribution to the attenuation uncertainty is negligible compared to other uncertainties and can be neglected. Then for 662 keV γ-rays passing through the lead sample, by Equations 3a and 3b,

$$\mu = -\frac{1}{(0.676\text{ cm})(11.34\text{ g}\cdot\text{cm}^{-3})}\ln\left(\frac{4160}{8870}\right) = 0.0988\text{ cm}^2\cdot\text{g}^{-1}$$

$$\delta_\mu = \frac{1}{(0.676\text{ cm})(11.34\text{ g}\cdot\text{cm}^{-3})}\sqrt{\left(\ln\left(\frac{4160}{8870}\right)\right)^2\left(\frac{0.100\text{ cm}}{0.676\text{ cm}}\right)^2+\left(\frac{181}{4160}\right)^2+\left(\frac{264}{8870}\right)^2}$$

$$= 0.016\text{ cm}^2\cdot\text{g}^{-1}$$

So lead has a mass attenuation coefficient of $0.099 \pm 0.016\text{ cm}^2\cdot\text{g}^{-1}$ at 662 keV. About 82% of the uncertainty in this attenuation is due to the uncertainty in the thickness of the lead. The lead had a relatively high uncertainty in its thickness compared to the aluminum and copper

samples because the lead sample thickness was not as uniform as the aluminum and copper. For measurements with a lower number of incident counts, the count components tend to contribute to most of the uncertainty, though, because the uncertainties in the thicknesses of the aluminum and copper absorbers are less than 5 percent.

This calculation follows in the same way for each of the other energies and each absorber material. Since two aluminum samples were tested, though, the average attenuation coefficient and its uncertainty were calculated by

$$\mu_{\text{avg}} = \frac{1}{N}\sum_{i=1}^{N}\mu_i \tag{4a}$$

$$\delta_{\mu_{\text{avg}}} = \frac{1}{N}\sqrt{\sum_{i=1}^{N}\delta_{\mu_i}^2} \tag{4b}$$

where N is the number of data values. For example, the two calculated aluminum attenuation coefficients at 662 keV were averaged:

$$\mu_{\text{avg}} = \frac{1}{2}(0.183 + 0.010)\ \text{cm}^2 \cdot \text{g}^{-1} = 0.0965\ \text{cm}^2 \cdot \text{g}^{-1}$$

$$\delta_{\mu_{\text{avg}}} = \frac{1}{2}\sqrt{(0.056)^2 + (0.071)^2}\ \text{cm}^2 \cdot \text{g}^{-1} = 0.045\ \text{cm}^2 \cdot \text{g}^{-1}$$

Thus, $\mu = \mu_{\text{avg}} = 0.097 \pm 0.045\ \text{cm}^2 \cdot \text{g}^{-1}$ for aluminum at 662 keV. The results of these calculations are given in Tables 3, 4 and 5 for aluminum, copper and lead, respectively.

Table 3 Aluminum absorber photon counts and mass attenuation coefficients. The incident intensity or counts without the absorber (minus the background) are given by $I - B$, and the residual intensity or counts with the absorber are given by $S - B$. The average attenuation, μ_{avg}, is calculated from each of the two aluminum absorbers tested.

Energy (keV)	Thickness (cm)	$I - B$	$S - B$	μ ($\text{cm}^2 \cdot \text{g}^{-1}$)	μ_{avg} ($\text{cm}^2 \cdot \text{g}^{-1}$)
31	0.313 ± 0.010	14873 ± 136	6390 ± 93	1.000 ± 0.067	1.038 ± 0.081
	0.635 ± 0.010	7270 ± 100	1149 ± 43	1.07 ± 0.15	
32	0.313 ± 0.010	321 ± 52	261 ± 43	0.24 ± 0.27	0.66 ± 0.27
	0.635 ± 0.010	228 ± 23	36 ± 13	1.08 ± 0.47	
81	0.313 ± 0.010	2081 ± 70	1945 ± 68	0.080 ± 0.058	0.214 ± 0.080
	0.635 ± 0.010	705 ± 49	388 ± 38	0.35 ± 0.15	
356	0.313 ± 0.010	3587 ± 138	3501 ± 137	0.029 ± 0.065	0.054 ± 0.057
	0.635 ± 0.010	2007 ± 113	1752 ± 96	0.079 ± 0.094	
662	0.313 ± 0.010	8870 ± 264	7599 ± 284	0.183 ± 0.056	0.097 ± 0.046
	0.635 ± 0.010	2746 ± 123	2699 ± 106	0.010 ± 0.071	
1173	0.313 ± 0.010	483 ± 58	394 ± 54	0.24 ± 0.22	0.13 ± 0.19
	0.635 ± 0.010	368 ± 73	357 ± 65	0.02 ± 0.32	
1332	0.313 ± 0.010	402 ± 66	302 ± 66	0.34 ± 0.32	0.19 ± 0.22
	0.635 ± 0.010	317 ± 57	299 ± 52	0.03 ± 0.30	

Table 4 Copper absorber photon counts and mass attenuation coefficients. The incident intensity or counts without the absorber (minus the background) are given by $I - B$, and the residual intensity or counts with the absorber are given by $S - B$. The 31 and 32 keV peaks were indistinguishable through the copper absorber and are excluded.

Energy (keV)	Thickness (cm)	$I - B$	$S - B$	μ ($\text{cm}^2 \cdot \text{g}^{-1}$)
81	0.630 ± 0.030	2081 ± 70	168 ± 26	0.446 ± 0.035
356	0.630 ± 0.030	3587 ± 138	2440 ± 120	0.068 ± 0.012
662	0.630 ± 0.030	8870 ± 264	5168 ± 249	0.096 ± 0.011
1173	0.630 ± 0.030	483 ± 58	138 ± 56	0.222 ± 0.076
1332	0.630 ± 0.030	402 ± 66	283 ± 52	0.062 ± 0.044

Table 5 Lead absorber photon counts and mass attenuation coefficients. The incident intensity or counts without the absorber (minus the background) are given by $I - B$, and the residual intensity or counts with the absorber are given by $S - B$. The 31 and 32 keV peaks were indistinguishable through the lead absorber and are excluded.

Energy (keV)	Thickness (cm)	$I - B$	$S - B$	μ ($\text{cm}^2 \cdot \text{g}^{-1}$)
81	0.676 ± 0.100	2081 ± 70	49 ± 19	0.489 ± 0.088
356	0.676 ± 0.100	3587 ± 138	697 ± 63	0.214 ± 0.034
662	0.676 ± 0.100	8870 ± 264	4160 ± 181	0.099 ± 0.016
1173	0.676 ± 0.100	483 ± 58	318 ± 49	0.055 ± 0.027
1332	0.676 ± 0.100	402 ± 66	212 ± 56	0.083 ± 0.042

Figure 2 shows the mass attenuation coefficients for aluminum, copper and lead over the range of energies tested in comparison to the reference data by McCrary *et al*. [3] and Conner *et al*. [4], while Figures 3 through 5 show the same attenuation coefficients on separate graphs for aluminum, copper and lead in comparison with the reference data.

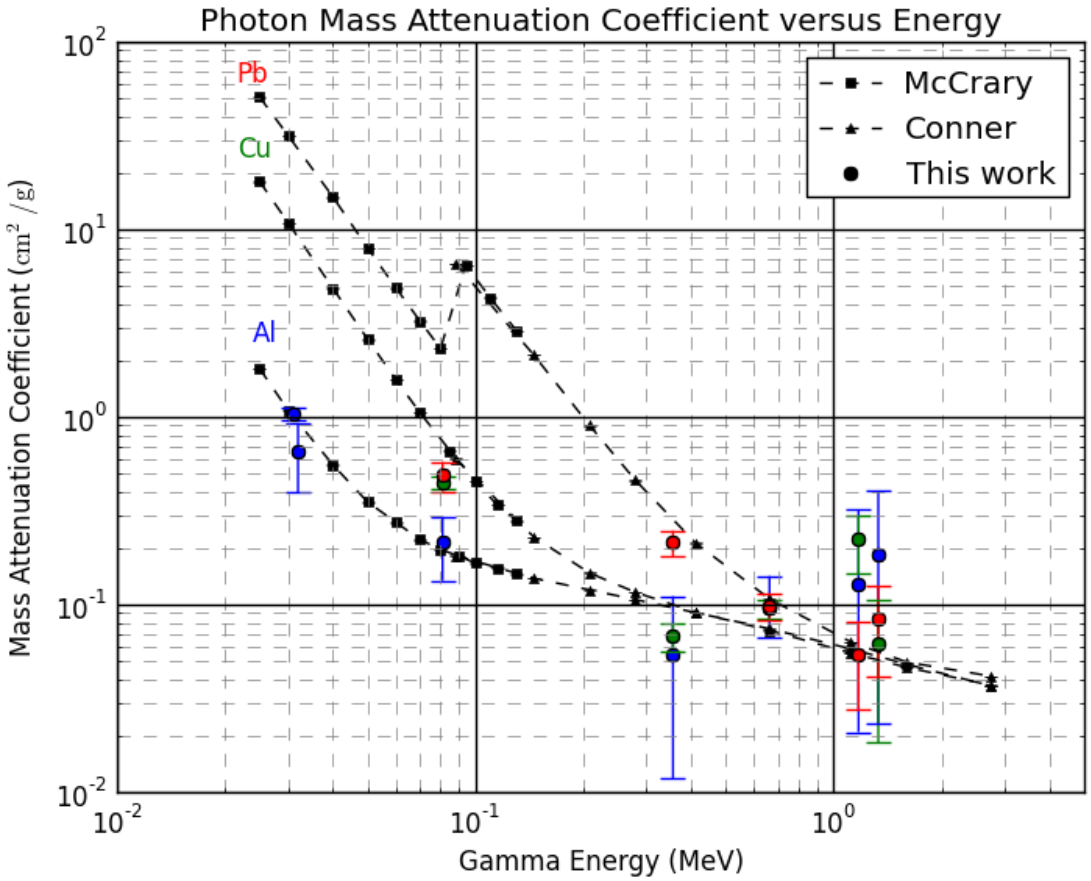

Figure 2 Graph of all photon mass attenuation coefficients versus incident γ-ray energy plotted against reference data. Aluminum, copper and lead are shown from bottom to top in blue, green and red, respectively. Reference data is connected by piecewise linear segments.

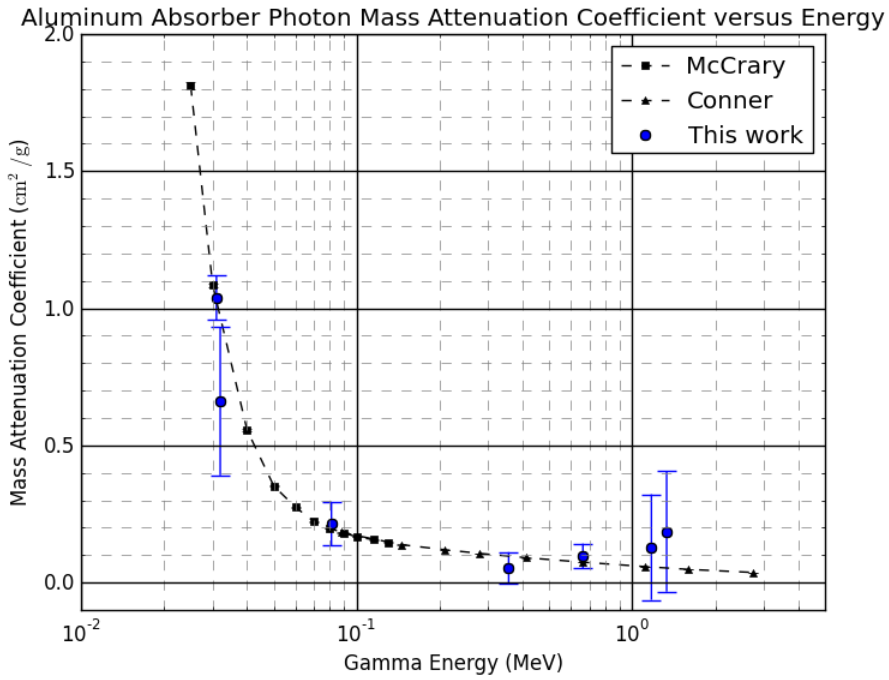

Figure 3 Aluminum attenuation coefficients. High uncertainties are mostly due to small counts. Some uncertainties were such that the lower error bar became negative, preventing a true typical log-log plot. Reference data is connected by piecewise linear segments.

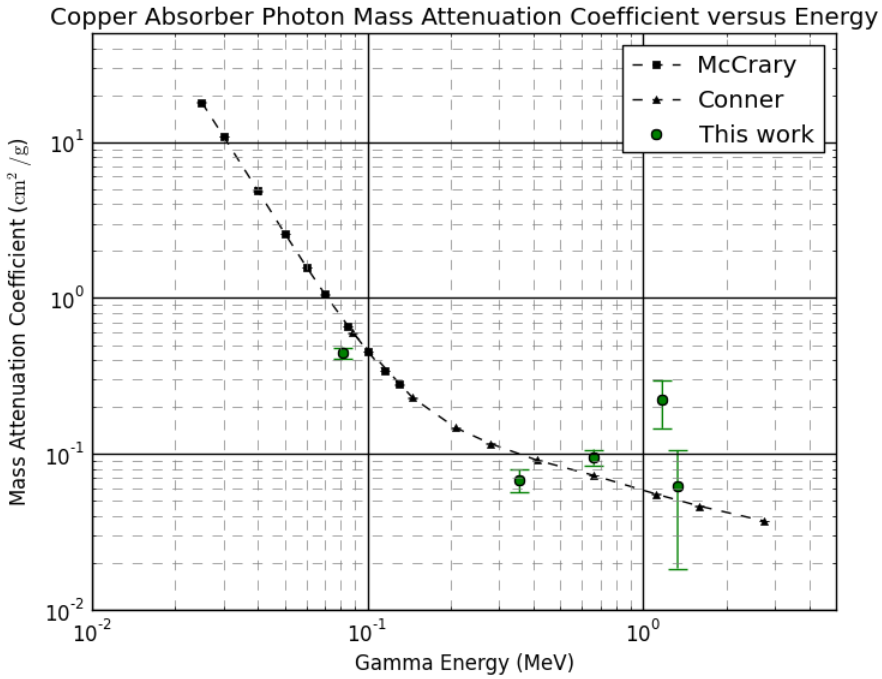

Figure 4 Copper attenuation coefficients. Reference data is connected by piecewise linear segments.

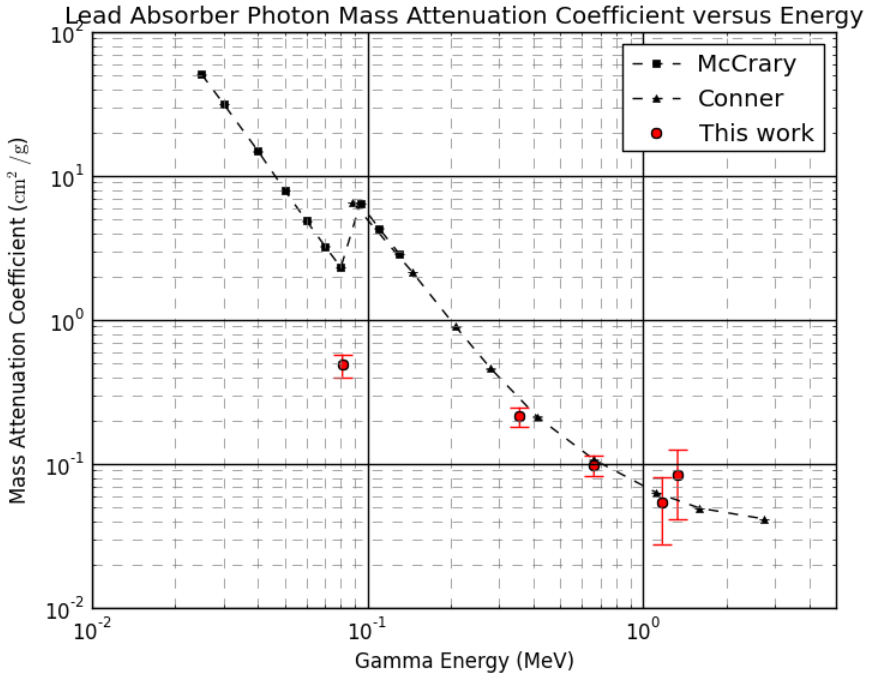

Figure 5 Lead attenuation coefficients. Reference data is connected by piecewise linear segments.

By performing a weighted cubic spline interpolation on the reference data, the reduced Chi-squared value was computed for each absorber according to

$$\bar{\chi}^2 = \frac{1}{N}\sum_{i=1}^{N}\left(\frac{\mu_i - \mu_{\text{fit}}(E_i)}{\delta_{\mu_i}}\right)^2 \tag{3}$$

where N is the number of points, $\mu_{\text{fit}}(E_i)$ is the interpolated value at the energy E_i for each μ_i with an uncertainty of δ_{μ_i}. Aluminum, copper and lead had reduced Chi-squared values of $\bar{\chi}^2_{\text{Al}} = 0.36$, $\bar{\chi}^2_{\text{Cu}} = 17$ and $\bar{\chi}^2_{\text{Pb}} = 101$, respectively.

Discussion and Conclusions

The reduced Chi-squared values give an overall indication of how well the attenuation coefficients compare to reference data by: $\bar{\chi}^2 \leq 1$ indicates close agreement to the expected values, whereas $\bar{\chi}^2 \gg 1$ indicates a significant disagreement. Then overall, the aluminum data agrees with the reference data, while the copper and lead data have an overall disagreement with

the reference data. Examining Figure 3, the close agreement of aluminum may be due to an overestimate of uncertainty for some attenuation coefficients, but most of the attenuations are within error of the reference data. On the other hand, examining Figures 4 and 5 reveal that only 20 and 60 percent of the points—in particular, the higher energy attenuation coefficients—are within error for copper and lead, respectively. This disagreement could be due to an underestimate of the errors in the lead and copper attenuation coefficients or due to uncertainty in the actual energy value of the γ-ray.

In general, the quality of the radiation sources and detector had the greatest impact on the accuracy and precision of the measurement. The low- and high-energy γ-rays from the Barium-133 and Cobalt-60 sources, respectively, were often difficult to distinguish and created uncertainty in both their counts and their actual energy—especially when measured through the copper and lead absorbers.

At 662 keV, only the copper was not within its uncertainty of the reference attenuation coefficient. The lead attenuation coefficient had the closest agreement with the reference value of $\mu_{\mathrm{Pb}} = 0.1074 \pm 0.0005$, with roughly 8% error, followed by aluminum at 30% ($\mu_{\mathrm{Al}} = 0.07436 \pm 0.00025$) and copper at 32% error ($\mu_{\mathrm{Cu}} = 0.07285 \pm 0.00038$) [4]. The 662 keV coefficients were comparatively close to the reference data most likely due to the relatively high strength of the Cesium-137 γ source (see Table 1), thus making it easier to identify the energy peak in the spectra.

In addition to the relative source strength, the peak widths are limited by the energy resolution of the detector (perhaps around 10% for a NaI scintillator); both of these factors make it difficult to analyze the energy spectra accurately and precisely. Since radiation counting is governed by Poisson statistics, the relative uncertainty in the counts decreases as the counts

increase. This would suggest that increasing the energy peak width or collection time to increase the counts would decrease relative uncertainty, but both of these actions introduce other uncertainties. Larger peak widths result in a larger uncertainty in the energy, and using a larger area in the analysis creates systematic error in the total number of counts because counts that are not from the actual energy of interest—possibly an inseparable peak—are noise that disrupts the data. Simply subtracting off the background spectra can help reduce counts due to noise, but there are still random variations in the background levels, and the finite width of the energy peaks due to the detector limitations can cause a blending in peaks that makes them inseparable. Although taking data for a longer time will have the benefit of producing more pronounced peaks with less relative uncertainty in their counts, the peaks will still not necessarily separate, resulting in a systematic error in the counts. So a somewhat arbitrary decision must be made in the spectra analysis to maximize the counts of the energy peak but minimize energy uncertainty and counts due to noise. Ultimately, typical energy peak widths used were roughly 10 to 30 percent of the peak energy.

Other sources of error are systematic errors like not calibrating the MCA properly, having a misaligned detector, or poorly collimated γ-ray beam. Improperly calibrating the MCA with reference spectra causes uncertainty in the energy values of the energy spectra. Non-uniform material thicknesses and material impurities also introduce errors in the measurement, but these uncertainties are generally small compared to the uncertainties in the counting statistics and can be minimized by measuring the attenuation several times over the area of each sample and using an impurity correction factor [4]. The alignment of the detector relative to the γ-beam and absorber or a poorly collimated beam can cause γ-rays that travel a distance through the absorber greater than its thickness ($d \propto x \sec\theta$) to come into the detector, since the γ-rays would travel at

an angle relative to the absorber's surface normal. Secondary interactions of the photons with the matter around the detector would also interfere with the attenuation measurement. With sufficient time and equipment, then, ensuring that the γ-beam is collimated and aligned properly with the detector would improve measurement accuracy.

According to Conner *et al*. [4], the most efficient use of counting time is made by selecting a material thickness such that the ratio of the residual beam intensity to the incident beam intensity is $0.1 \leq \frac{S-B}{I-B} \leq 0.4$. Thus, in an attempt to decrease some of the low Z aluminum sample ratios—all but one of which were greater than 0.75—a thicker aluminum sample was tested. Interestingly, increasing the aluminum absorber thickness actually increased the ratio for three of the energies tested (662, 1173 and 1332 keV) to nearly 1, which may be due to poor analysis of the energy peak counts with the absorber, but the relative error in the attenuation coefficient did not improve for only two energies (7 and 20 percent increases in relative error at 31 and 81 keV, respectively). Improvements ranged from 50 percent decrease in relative error at the low- to mid-energy range up to 500 percent decrease for the higher Cobalt-60 energies. Thus, the thicker absorber (and the average of the two absorbers) had better agreement with the reference data. Ideally, this procedure of trying to find an absorber that fits this ratio could be repeated and the attenuation coefficients averaged for each of the materials.

It is difficult to characterize an overall trend of the data for each absorber and to compare them to each other for a given energy, due to the relatively high uncertainties and fluctuations. However, at energies above 662 keV, the discrepancies between the attenuations of each absorber are within the aluminum absorber attenuation uncertainty. Thus, at the energies tested between 662 keV and 1332 keV, the absorption coefficients appear to be roughly material-independent, indicating that Compton scattering is the dominant scattering mechanism in this

energy range. Similarly, since the attenuation coefficient is material-dependent at energies below 662 keV, the photoelectric effect is the dominant absorption mechanism. This is in close agreement with Figure 6. The energy range tested was not high enough for pair production to have any significant effect.

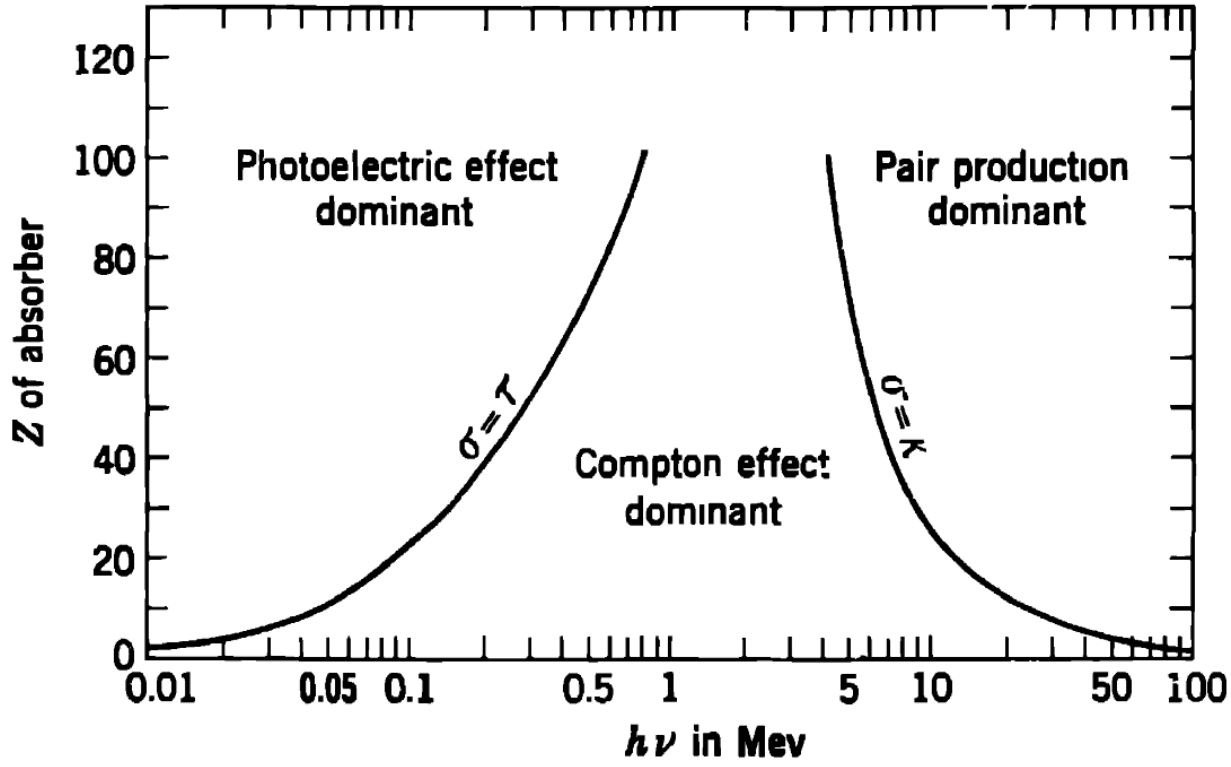

Figure 6 Relative importance of the three major types of γ-ray interactions [2]. The lines show the values of Z and $h\nu$ for which the two neighboring effects are just equal.

Summary

There was a good agreement between the measured photon mass attenuation coefficients for aluminum absorber over the energy range tested and the reference data, while the copper and lead absorber coefficients did not agree with reference values. The attenuation coefficients of all three absorbers at and above 662 keV were within the uncertainty of the aluminum absorber coefficient, which indicates that Compton scattering was the dominant photon-matter interaction in this region, due to its independence of Z. Better accuracy in the coefficients can be achieved

by repeating the measurement for each sample and each energy several times, ensuring that the γ beam is well-collimated and using good quality radiation sources.

References

[1] Photon Attenuation Experiment Lab Manual.
[2] R. D. Evans, *The Atomic Nucleus* (McGraw-Hill, New York, 1955), p. 711-713.
[3] J. H. McCrary, E. H. Plassmann, J. M. Puckett, A. L. Conner, and G. W. Zimmermann, *Phys. Rev*. **153**, 307 (1967).
[4] A. L. Conner H. F. Atwater, and E. H. Plassmann, *Phys. Rev*. **A1**, 539 (1970).

Appendix: Uncertainty in the attenuation coefficient

The uncertainty in the mass attenuation coefficient is given by the components of the uncertainty added in quadrature:

$$\delta_\mu = \sqrt{\left(\frac{\partial\mu}{\partial x}\right)^2 \delta_x^2 + \left(\frac{\partial\mu}{\partial\rho}\right)^2 \delta_\rho^2 + \left(\frac{\partial\mu}{\partial(S-B)}\right)^2 \delta_{S-B}^2 + \left(\frac{\partial\mu}{\partial(I-B)}\right)^2 \delta_{I-B}^2}$$

$$= \sqrt{\left(\frac{1}{x^2\rho}\ln\left(\frac{S-B}{I-B}\right)\right)^2 \delta_x^2 + \left(\frac{1}{x\rho^2}\ln\left(\frac{S-B}{I-B}\right)\right)^2 \delta_\rho^2 + \left(\frac{1}{(S-B)x\rho}\right)^2 \delta_{S-B}^2 + \left(\frac{1}{(I-B)x\rho}\right)^2 \delta_{I-B}^2}$$

$$= \frac{1}{x\rho}\sqrt{\left(\ln\left(\frac{S-B}{I-B}\right)\right)^2 \left(\left(\frac{\delta_x}{x}\right)^2 + \left(\frac{\delta_\rho}{\rho}\right)^2\right) + \left(\frac{\delta_{S-B}}{S-B}\right)^2 + \left(\frac{\delta_{I-B}}{I-B}\right)^2}$$

In the taking the average of N attenuation coefficients, the uncertainty is given by

$$\delta_{\mu_{\text{avg}}} = \sqrt{\sum_{i=1}^{N}\left(\frac{\partial\mu_{\text{avg}}}{\partial\mu_i}\right)^2 \delta_{\mu_i}^2} = \sqrt{\sum_{i=1}^{N}\left(\frac{1}{N}\right)^2 \delta_{\mu_i}^2} = \frac{1}{N}\sqrt{\sum_{i=1}^{N}\delta_{\mu_i}^2}$$